Supplemental Document

Optics Letters

Spectral caustics of high-order harmonics in one-dimensional periodic crystals: supplement

JIAXIANG CHEN,[1] QINZHI XIA,[2,3] AND LIBIN FU[1,4]

[1]*Graduate School of China Academy of Engineering Physics, No. 10 Xibeiwang East Road, Haidian District, Beijing, 100193, China*
[2]*Institute of Applied Physics and Computational Mathematics, Beijing 100088, China*
[3]*e-mail: xia_qinzhi@iapcm.ac.cn*
[4]*e-mail: lbfu@gscaep.ac.cn*

Supplement DOI: https://doi.org/10.6084/m9.figshare.14396054

Parent Article DOI: https://doi.org/10.1364/OL.423940

Spectral caustics of high-order harmonics in one-dimensional periodic crystals: supplementary material

In Sec. 1, we present the derivation of the Hessian matrix of classical action. In Sec. 2, we make a series of extensive calculations to investigate Fig. 2 in the main text, including the effects of dephasing time, the variant of the transition dipole moment, and the pulse duration on the high order harmonic spectrum.

1. DERIVATIONS OF THE HESSIAN MATRIX

The time-dependent schrödinger equation (TDSE) in length gauge is given by

$$i\partial_t\psi(x,t) = [H_0 - xF(t)]\,\psi(x,t), \tag{S1}$$

where $F(t)$ is the external field, $H_0 = \hat{p}^2/2 + V(x)$ is the field-free Hamiltonian and $V(x)$ is the periodic potential. The eigenvalue equation of the field-free Hamiltonian is given by $H_0\phi_n(k,x) = \varepsilon_n(k)\phi_n(k,x)$, where $\varepsilon_n(k)$ and $\phi_n(k,x)$ are the eigenenergy and the corresponding Bloch state of crystal momentum k, respectively. Expanding the wavefunction $\psi(x,t)$ as $\psi(x,t) = \sum_n \int_{BZ} \mathrm{d}k\; a_n(k,t)\phi_n(k,x)$ and substituting it into Eq. (S1), we have the semiconductor Bolch equations (SBEs) as

$$\begin{aligned} i\partial_t\rho_{nn'}(K,t) = &-\left(\varepsilon_n(K+A(t)) - \varepsilon_{n'}(K+A(t)) + i\frac{(1-\delta_{nn'})}{T_2}\right)\rho_{nn'}(K,t) \\ &+ F(t)\sum_m (d_{mn}(K+A(t))\rho_{mn'}(K,t) - d_{n'm}(K+A(t))\rho_{nm}(K,t)), \end{aligned} \tag{S2}$$

where $\rho_{nn'}(K,t) = a_n^*(K,t)a_{n'}(K,t)$, $d_{nn'}(k) = -i\,p_{nn'}(k)/\left[\varepsilon_n(k) - \varepsilon_{n'}(k)\right]$ is the transition dipole moment, and $p_{nn'}(k) = \langle\phi_n(k)|\hat{p}|\phi_{n'}(k)\rangle$. T_2 is introduced as the dephasing time. Here, we use a transformation $k = K + A(t)$, where $A(t) = -\int_{-\infty}^{t} F(\tau)\mathrm{d}\tau$ is the vector potential. Hence, the interband current is $J_{er}(t) = -\int_{BZ}\mathrm{d}K\sum_{n,n';n\neq n'}\rho_{nn'}(K,t)p_{nn'}(K+A(t))$, and the intraband current is $J_{ra}(t) = -\int_{BZ}\mathrm{d}K\sum_n \rho_{nn}(K,t)p_{nn}(K+A(t))$.

With a transformation $a_n(K,t) = b_n(K,t)\exp\left(-i\int_{-\infty}^{t}\varepsilon_n(K+A(\tau))d\tau\right)$ [1], the two band SBEs can be rewritten as

$$\begin{aligned} \dot{\pi}(K,t) &= -\frac{\pi(K,t)}{T_2} - iF(t)d(K+A(t))(n_v - n_c)e^{-iS(K,t)}, \\ \dot{n}_m(K,t) &= is_m F(t)d(K+A(t))\pi(K,t)e^{iS(K,t)} + c.c, \end{aligned} \tag{S3}$$

where $S(t) = \int_{-\infty}^{t}\varepsilon_c(K+A(\tau)) - \varepsilon_v(K+A(\tau))d\tau$ and $d(k) = -i\,p_{cv}(k)/\varepsilon_g(k)$. $n_m(K+A(t)) = |b_m(K+A(t))|^2$ and $\pi(K+A(t)) = b_c^*(K+A(t))b_v(K+A(t))$ are the diagonal and off-diagonal elements of the density matrix, respectively. $s_m = -1$ and 1 for m =v (valence band), and c(conduction band), respectively. Assuming $n_v - n_c \approx 1$, the interband harmonics can be expressed as $J_{er}(\omega) = \int_{BZ}dk\int_{-\infty}^{\infty}dt\int_{-\infty}^{t}dt'\,g(k,t',t)e^{-iS(k,t',t)+i\omega t-(t-t')/T_2} + c.c.$, where $S(k,t',t) = \int_{t'}^{t}\varepsilon_c(K+A(\tau)) - \varepsilon_v(K+A(\tau))d\tau$. Similar to the treatment in the original recollision model[1], we assume that $g(k,t',t) = \omega d(k)d^*(k+A(\tau)-A(t))$ is a slowly varying term. Applying the stationary phase method to the integration, we get the saddle point equations as

$$\frac{\partial S}{\partial k} = \int_{t'}^{t}\frac{\partial\varepsilon_g(\kappa_\tau)}{\partial k}d\tau = x_c - x_v = 0, \tag{S4a}$$

$$\frac{\partial S}{\partial t'} = -\varepsilon_g(\kappa_{t'}) = 0, \tag{S4b}$$

$$\frac{\partial S}{\partial t} = \varepsilon_g(k) + F(t)\int_{t'}^{t}\frac{\partial\varepsilon_g(\kappa_\tau)}{\partial k}d\tau = \omega, \tag{S4c}$$

where $\kappa_\tau = k + A(\tau) - A(t)$.

As a result, the determinant of the Hessian matrix S'' can be expressed as

$$
\begin{aligned}
|S''| &= \begin{bmatrix}
\int_{t'}^{t} \frac{\partial^2 \varepsilon_g(\kappa_\tau)}{\partial k^2} d\tau & -\frac{\partial \varepsilon_g(\kappa_{t'})}{\partial k} & \frac{\partial \varepsilon_g(k)}{\partial k} + F(t) \int_{t'}^{t} \frac{\partial^2 \varepsilon_g(\kappa_\tau)}{\partial k^2} d\tau \\
-\frac{\partial \varepsilon_g(\kappa_{t'})}{\partial k} & F(t') \frac{\partial \varepsilon_g(\kappa_{t'})}{\partial k} & -F(t) \frac{\partial \varepsilon_g(\kappa_{t'})}{\partial k} \\
\frac{\partial \varepsilon_g(k)}{\partial k} + F(t) \int_{t'}^{t} \frac{\partial^2 \varepsilon_g(\kappa_\tau)}{\partial k^2} d\tau & -F(t) \frac{\partial \varepsilon_g(\kappa_{t'})}{\partial k} & F(t) \frac{\partial \varepsilon_g(k)}{\partial k} + F^2(t) \int_{t'}^{t} \frac{\partial^2 \varepsilon_g(\kappa_\tau)}{\partial k^2} d\tau
\end{bmatrix} \\
&= \begin{bmatrix}
b & -a(\kappa_{t'}) & a(k) + F(t) b \\
-a(\kappa_{t'}) & F(t') a(\kappa_{t'}) & -F(t) a(\kappa_{t'}) \\
a(k) + F(t) b & -F(t) a(\kappa_{t'}) & F(t) a(k) + b F^2(t)
\end{bmatrix} \\
&= \begin{bmatrix}
b & -a(\kappa_{t'}) & a(k) + F(t) b \\
-a(\kappa_{t'}) & F(t') a(\kappa_{t'}) & -F(t) a(\kappa_{t'}) \\
a(k) & 0 & 0
\end{bmatrix} \\
&= a(k) a(\kappa_{t'}) \left[a(\kappa_{t'}) F(t) - (a(k) + b F(t)) F(t') \right],
\end{aligned}
\tag{S5}
$$

where $a(\kappa_\tau) = \frac{\partial \varepsilon_g(\kappa_\tau)}{\partial k}$,and $b = \int_{t'}^{t} \frac{\partial^2 \varepsilon_g(\kappa_\tau)}{\partial k^2} d\tau$.

From Eq. (S4c), we can obtain

$$
\frac{d\omega}{dt'} = -a(\kappa_{t'}) F(t) + \left[a(k) + b F(t) \right] \frac{dk}{dt'} + \left[a(k) + b F(t) \right] F(t) \frac{dt}{dt'}. \tag{S6}
$$

Taking the derivative of Eq. (S4b) in the t' direction, we can get

$$
\frac{dk}{dt'} = -F(t) \frac{dt}{dt'} + F(t'). \tag{S7}
$$

According to Eq. (S6) and Eq. (S7),

$$
\frac{d\omega}{dt'} = \left[a(k) + b F(t) \right] F(t') - a(\kappa_{t'}) F(t), \tag{S8}
$$

so that the determinant of the Hessian matrix [see Eq. (S5)] reduces to

$$
\left| S'' \right| = -a(k) a(\kappa_{t'}) \frac{d\omega}{dt'}. \tag{S9}
$$

2. EXTENSIVE CALCULATIONS

This section makes a series of extensive calculations to investigate the HHG patterns in Fig. 2. For better comparison, we plot Fig. 2 in the first column of Fig. S1. These results are obtained by solving the time-dependent Schrödinger equation in the velocity gauge [VG-TDSE, Eq. (6) in the main text] with a laser pulse duration of $T_p = 11\, T_0$, where T_0 is an optical cycle.

Firstly, to study the difference between the velocity and length gauges, we also solve the length gauge two-band semiconductor Bolch equations (LG-SBEs, Eq. (S2)). The band structure and the transition dipole moment are extracted from the one-dimensional model used in the main text. Different dephasing time T_2 are applied here, i.e., $T_2 = \infty$ (the second column of Fig. S1), $T_2 = T_0$ (the third column), and $T_2 = T_0/2$ (the fourth column), respectively. Comparing the HHG spectra for the velocity (the first column) and length (the second column) gauges, the primary pattern of the HHG remains the same in different gauges, while some minor differences may be ascribed to the neglect of the higher bands in the case of the length gauge. The second, third, and fourth columns show that the branch from the bottom left to the top right of the caustic pattern becomes weaker with the decrease of T_2. This branch corresponds to the coalescence of two long trajectories. In contrast, the caustic structures generating by the coalescence of the two short trajectories remain sharp.

Second, we investigate the variant of the interband transition dipole moment. In the simulation of the fifth column, we by-hand set interband transition dipole moment $d(k)$ constantly equals $d(0)$. We find that the structure and position of the major enhancement we focus on in this work

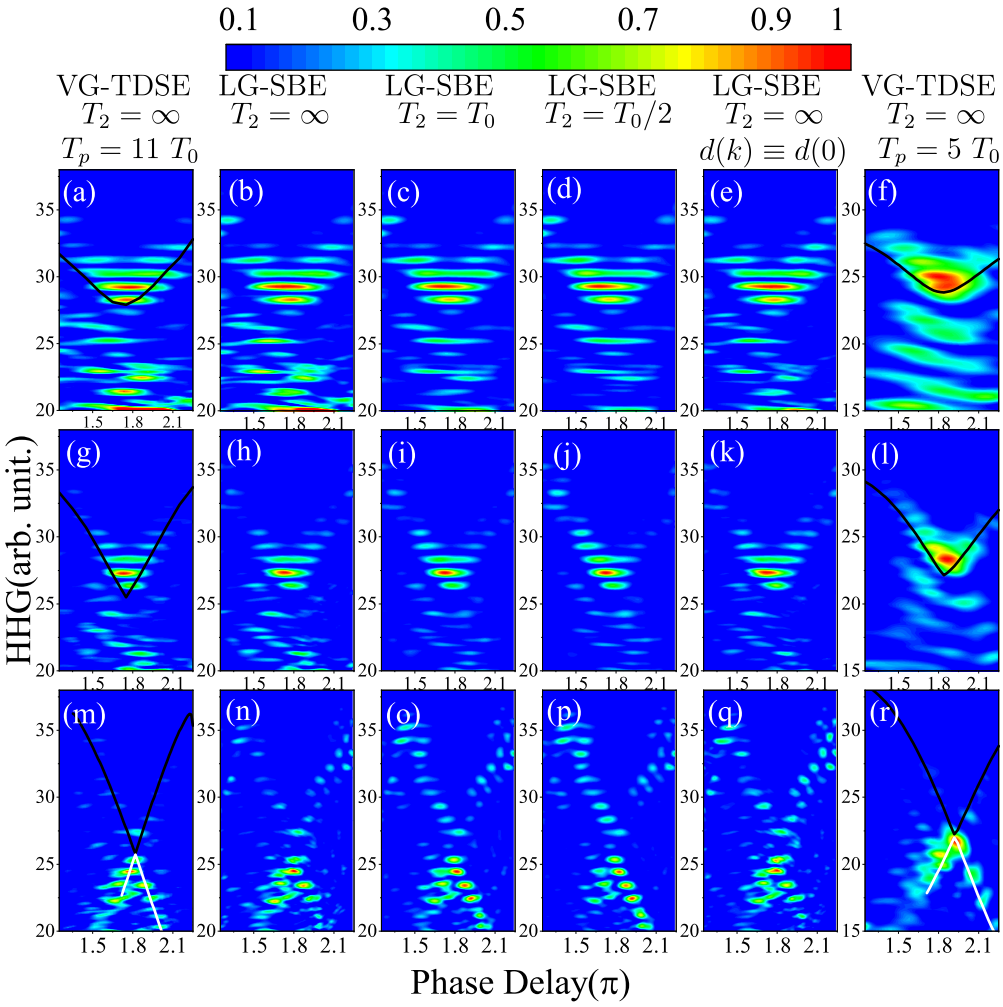

Fig. S1. Normalized HHG spectra as a function of the phase delay φ for $R \approx 0.29$ [(a)-(f), the first row], $R \approx 0.49$ [(g)-(l), the second row] and $R \approx 0.93$ [(m)-(r), the third row], respectively. [(a),(g),(m), the first column] Reproduction of Fig. 2 changing the alignment. HHG spectra with dephasing time $T_2 = \infty$ (the second column), $T_2 = T_0$ (the third column) and $T_2 = T_0/2$ (the fourth column) by solving the SBEs in the length gauge. [(e),(k),(q), the fifth column] The same as (b), (h), (n) [the second column] except that $d(k)$ is fixed at $d(0)$. [(f),(l),(r), the sixth column] Spectra by solving the TDSE in the velocity gauge [Eq. (6) in the main text] with laser pulse duration of $T_p = 5\,T_0$. Black and white solid lines in the first and sixth columns are the caustic lines predicted by semi-classical theory.

remain the same as the results in the second column, where the transition dipole moment $d(k)$ is extracted from the 1D model in the main text and has a pronounced maximum at $k = 0$.

We also notice that, in Fig. S1(a) [Fig. 2(a) in the main text] and Fig. S1(g) [Fig. 2(b) in the main text], some secondary enhancements below the primary enhancement can be seen. In the second and third columns, the secondary enhancement is weaker due to the dephasing effect. More interestingly, in the fifth column, some secondary enhancements disappear when the dipole moment is by-hand set to be a constant. It suggests the relation between the secondary enhancement and the trajectories with non-zero electron-hole separation proposed recently [2–4].

Finally, we solve VG-TDSE with a shorter pulse duration, i.e., $T_p = 5\,T_0$, and plot the results in the sixth column. Different from the discrete structures in the first column, the patterns here are more continuous and easier to distinguish the caustic structures. Additionally, the structure and the position of the secondary enhancement change with the laser pulse duration.

REFERENCES

1. Vampa, G. and McDonald, C. R. and Orlando, G. and Klug, D. D. and Corkum, P. B. and Brabec, T., "Theoretical Analysis of High-Harmonic Generation in Solids," Phys. Rev. Lett. **113**,073901 (2014).
2. Osika, Edyta N. and Chacón, Alexis and Ortmann, Lisa and Suárez, Noslen and Pérez-Hernández, Jose Antonio and Szafran, Bartłomiej and Ciappina, Marcelo F. and Sols, Fernando and Landsman, Alexandra S. and Lewenstein, Maciej, "Wannier-Bloch Approach to Localization in High-Harmonics Generation in Solids," Phys. Rev. X **7**,021017 (2017).
3. Yue, Lun and Gaarde, Mette B., "Imperfect Recollisions in High-Harmonic Generation in Solids," Phys. Rev. Lett. **124**,153204 (2020).
4. Parks, A. M. and Ernotte, G. and Thorpe, A. and McDonald, C. R. and Corkum, P. B. and Taucer, M. and Brabec, T., "Wannier quasi-classical approach to high harmonic generation in semiconductors," Optica **7**,1764 (2020).